Downloaded from UvA-DARE, the institutional repository of the University of Amsterdam (UvA)
http://dare.uva.nl/document/169122

File ID	169122
Filename	Chapter 6: Atom chip loading and diagnostics

SOURCE (OR PART OF THE FOLLOWING SOURCE):

Type	Dissertation
Title	Permanent magnetic atom chips
Author	I. Barb
Faculty	Faculty of Science
Year	2010
Pages	viii, 90
ISBN	978-90-5776-207-9

FULL BIBLIOGRAPHIC DETAILS:
http://dare.uva.nl/record/335649

Copyright

It is not permitted to download or to forward/distribute the text or part of it without the consent of the author(s) and/or copyright holder(s), other then for strictly personal, individual use.

UvA-DARE is a service provided by the library of the University of Amsterdam (http://dare.uva.nl)

Chapter 6

Atom chip loading and diagnostics

In the previous chapters we have shown how one can use millimeter-scale permanent magnetic structures to create high-gradient traps for neutral atoms, and described how to fabricate such devices.

In this chapter we describe the loading and in-trap analysis of ultracold atom clouds confined using such a self-biased fully permanent magnet atom chip. Efficiently transferring atoms to the self-biased trap turned out to be nontrivial. In addition traditional analysis techniques, such as ballistic expansion, are complicated due to the presence of large magnetic field gradients. A major part of this work is in overcoming these difficulties.

6.1 Loading the Ioffe-Pritchard magnetic trap

To load the permanent magnet trap we adiabatically transfer the atoms from the spherical quadrupole trap by applying a combination of bias fields to the field of the permanent magnetic structure, the chip gradients being dominant. By applying a uniform bias field the magnetically trapped atoms change their position in space by shifting several millimeters toward the atom chip. Once the cloud is close enough to the chip, so that it feels its gradient, the atoms will be trapped in the magnetic field of the chip.

During the loading it is important to avoid regions of zero field. It is also important to avoid unwanted splitting of the trap during the transport of the cloud to the final trap. More about possible constraints can be found in [77]. The B-field trajectory that we used to load the atoms has been calculated with Mathematica, see Figure 6.1.

The loading can be explained as follows: We start with the initial coil based quadrupole trap, explained in the previous chapter, located 8 mm below the chip surface. At this moment we have two magnetic field minima: one weak trap created by the external coils, filled with atoms, and a tighter empty trap close to the chip surface, created by the permanent magnetic structure. There are

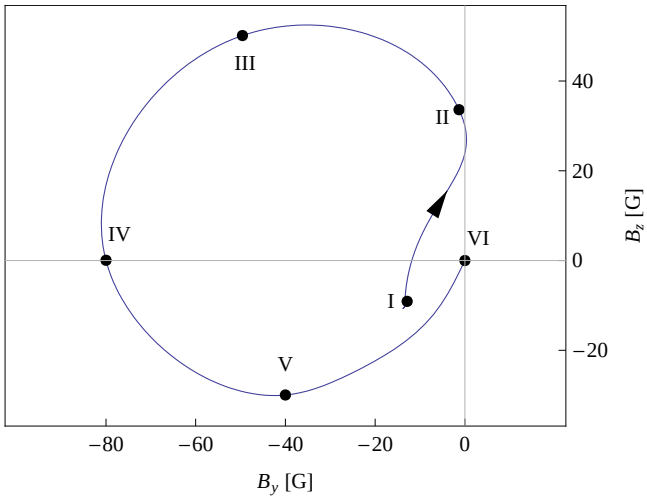

Figure 6.1: Calculated B-field trajectory used during the loading process. We start with the initial coil based quadrupole trap - position I. The magnetic quadrupole is then moved closer to the chip and turned off at position II. At this moment the trap turns into a Ioffe trap. This trap is then moved towards the final location, replacing the empty self-biased trap. At position VI all fields are switched off.

two ways of transferring the atoms between these two traps. One is to apply a uniform field in the y-direction reducing the separation between the two minima, merging them into a single hexapole trap. By the time the y field is switched off, the hexapole trap splits in two, leaving some atoms in the self-biased trap. The efficiency of this method is very low, therefore we choose the method described below.

The better way to transfer the atoms to the permanent magnetic trap is to exchange the two traps. This is done by applying uniform magnetic fields in the y and z-directions, as shown in Table 6.1, as well as Figure 6.1 (quoted in currents for convenience. Conversions from Amps to G, see Table 3.3). Also three-dimensional calculations of the magnetic field iso-surfaces during the loading are shown in Figure 6.2 II–VI. During the transfer the magnetic field gradient of the trap increases from 60 G/cm to 6800 G/cm which leads to significant heating of the cloud. At a certain point, the two field minima pass each other separated by a finite potential barrier of $\sim$ 15 G and hot atoms spill over to the decompressed trap. This loss mechanism takes away up to 80% of the atoms. In spite of this loss it is possible to load 2×10^6 atoms into the permanent magnet trap. A series of absorption images at various detunings are taken during the loading of the trapped cloud and are shown in Figure 6.2 a–e. The measured atom distributions compare very well with the calculated field distributions in Figure 6.2 II–VI. The cloud temperature inferred from the spectra in the self-biased trap is approximately 1 mK.

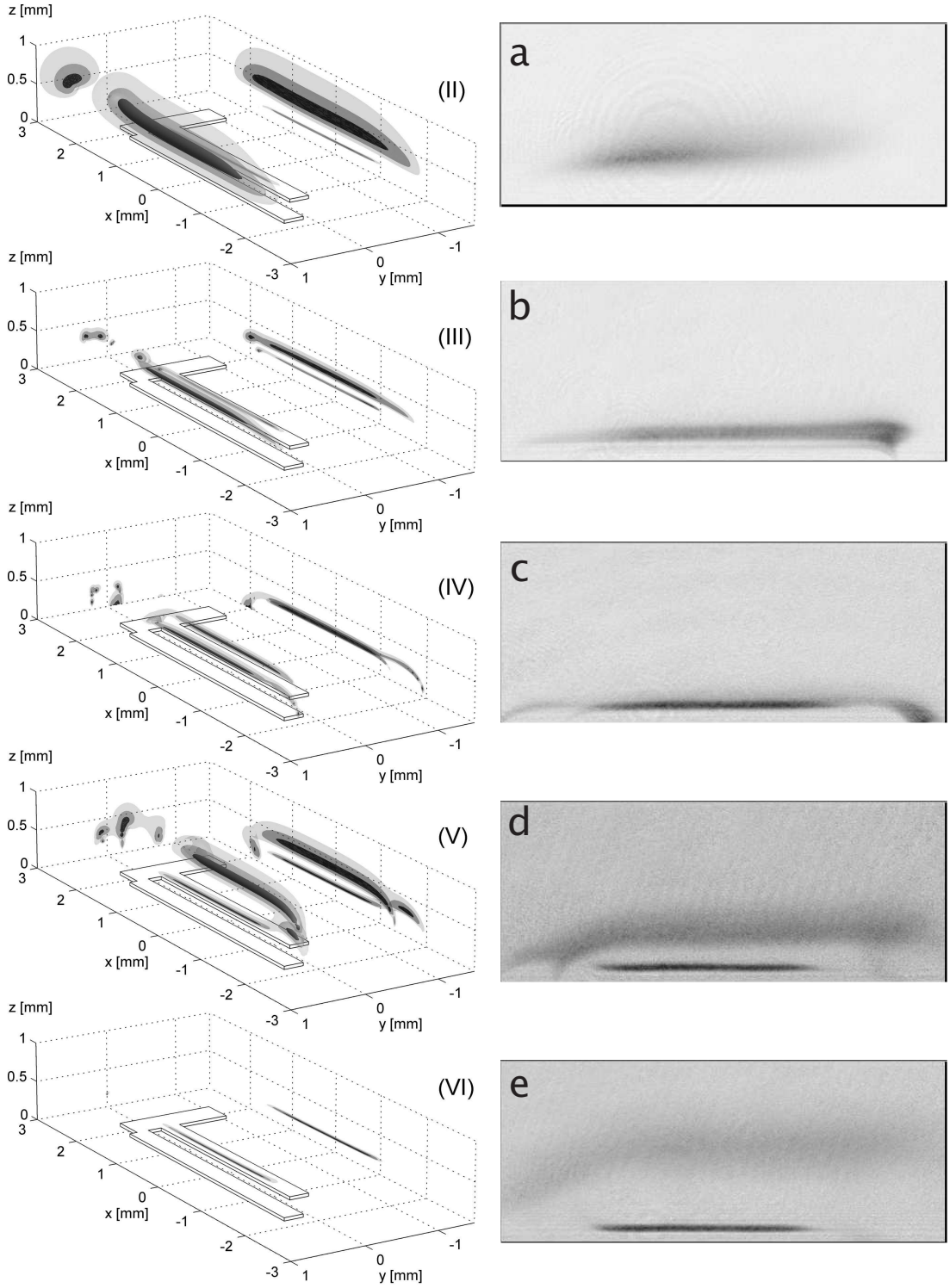

Figure 6.2: Atom chip loading - comparison of calculations and measurements. Figures (II - VI) show calculated contours of magnetic field strength together with their y and z - projections during the loading process. The figures correspond to positions (II - VI) in figure 6.1. Figures (a-e) represent absorption images taken during the loading process. Each image is composed of several absorption images taken at 22 different probe detunings, ranging from 0 to 60 MHz.

loading steps	time(ms)	magnetic coils	coils current	ramping time(ms)
1st step	200	Big coils	0 A	250
		MOT coil 1	-6.37 A	250
		MOT coil 2	6.37 A	250
2nd step	250	Big coils	5.95 A	60
		MOT coil 1	-5.1 A	60
		MOT coil 2	5.1 A	60
		MT coil 1	0.3 A	60
		MT coil 2	0.3 A	60
3rd step	60	Big coils	5.21 A	50
		MOT coil 1	-0.64 A	50
		MOT coil 2	0.64 A	50
4th step	50	Big coils	3.72 A	10
		MOT coil 1	0 A	10
		MOT coil 2	0 A	10
5th step	10	Big coils	1.41 A	2
		MOT coil 1	0.32 A	2
		MOT coil 2	0.32 A	2
6th step	2	Big coils	0 A	2
		MOT coil 1	0 A	2
		MOT coil 2	0 A	2

Table 6.1: The external coils currents schedule required to load the permanent magnetic structure. Note: bias fields are not quoted in Gauss, but in A required to produce the field. Quoting in amps is more convenient since we can measure the computer controlled currents more accurately. Conversion factors can be found in Table 3.3

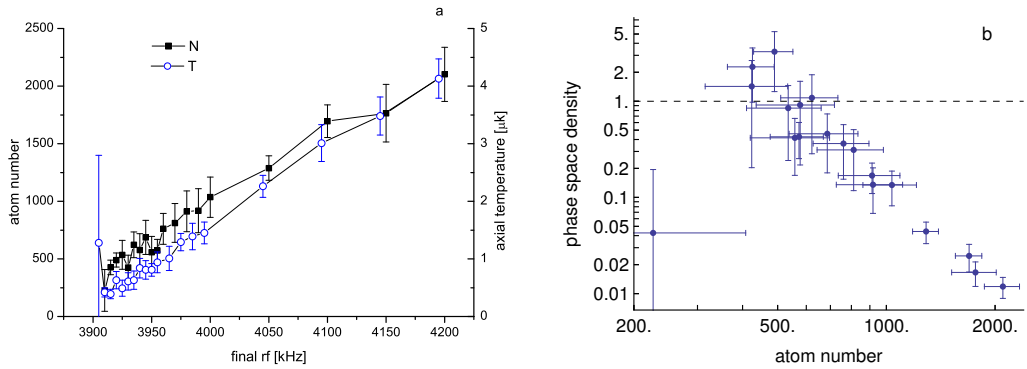

Figure 6.3: (a) Temperature (open square, T) and atom number (full square, N) inferred from the axial density distribution and (b) phase space density as a function of atom number. The dashed line marks the quantum degeneracy transition.

6.2 Measuring the atom number and temperature

Because we measure $in-situ$ and therefore in the presence of magnetic field, the atoms experience a position dependent Zeeman shift. Furthermore, we had to take into consideration the polarization of the probe light (see Chapter 5, section 5.1.3). For this we measured the full spectra by taking absorption images at different probe detunings. The probe was tuned over the range 0−60 MHz above resonance. Two dimensional atomic column density distribution from the absorption images is integrated radially to get a linear axial column density distribution. For cloud temperatures well above the critical temperature, the axial linear density distribution (atoms/m) is given by:

$$\rho(x) = N\omega\sqrt{\frac{m}{2\pi kT}}e^{-\frac{m\omega^2x^2}{2kT}} \tag{6.1}$$

where ω is the axial trap frequency and N the total atom number. Since the axial trap frequency is known, this fit can give both the temperature and the number of atoms in the cloud. When cooling down the cloud we observed that the radial cloud size is smaller than the pixel size. This effect would cause an underestimate of the observed optical density. Therefore, to measure the number of atoms we lift the magnetic field at the trap bottom by applying a 50 G magnetic field in the y-direction to relax the confinement. In addition, we blue detune the probe laser by 12 MHz. Lifting the trap would move the cloud out of focus, causing lensing [83] effects that can affect the observed cloud width. The cloud appears to have bright or dark halos around it, depending on the sign of the detuning. These effects are eliminated by taking absorption images over a range of 20 MHz above and below resonance and changing the position of the second lens of the imaging

telescope. The optimal lens position is found when these halo effects vanish.

In Figure 6.3 (a) we show the temperature inferred from the axial density distribution for various final frequencies above the trap bottom [84]. We have actually reached the transition temperature. At this temperature the fitting model breaks down and bimodal fitting will be required. During the final cooling process the phase-space density increased to PSD > 1, [85] reaching the degeneracy, as one can see in Figure (6.3 (b)). The observation of a BEC was done using different techniques like rf spectra and ejection of the clouds. An extensive description on how this has been done can be found in [14, 86].

6.2.1 Lifetime of the Ioffe trap - Majorana losses

The lifetime of the trap depends on the value of the magnetic field B_0 in the trap center. This field was measured by repetitively applying a radio frequency pulse for a duration of 0.5 ms, chosen to be short compared to the cloud thermalization time, and lowering the frequency until all atoms are removed from the trap.

The pressure in the science chamber is $\sim 4.5 \times 10^{-11}$ mbar, therefore long life times can be expected. However, when the adiabaticity condition is not fulfilled, which means that the magnetic moment of the atoms can not follow the magnetic field, spin flips into untrapped states can occur. We observed that increasing B_0 to a value of 2 G leads to an increase of the observed lifetime from 200 ms to about 12 s. The short lifetime (200 ms) can be due to the fact that the potential exhibits a pair of field zeroes rather than being a Ioffe trap. This can be attributed to the coarseness of the magnetic structure or inhomogeneity of the magnetization. The field zeroes were lifted by placing a permanent magnet on the optical table.

6.2.2 Measurement of the trap frequencies

A preliminary evaporative cooling stage is done before measuring the trap frequencies. This consists of a 10 s linear rf ramp from 35 MHz to 2 MHz. After the cloud is cooled to $\sim 1\mu$K we switch off the rf-cooling. The axial and radial oscillations of the cloud are driven by displacing the center of the trapping potential by means of the external coils. Before an image is taken we raise the bottom of the trap so the cloud gets bigger and easier to detect.

Axial frequency

To measure the axial frequency we excite the oscillation by applying a magnetic field in the x-direction. This leads to a center-of-mass oscillation of the cloud around its equilibrium position. The cloud is then let to oscillate in the trap for a variable holding time. In Figure 6.4 (a) we plot the cloud position versus time. We also analyzed the data using a fast Fourier transform (see Figure 6.4 (b)), which yielded a clear peak at a frequency of $\omega_a = 2\pi \times 128$ Hz. This is not in

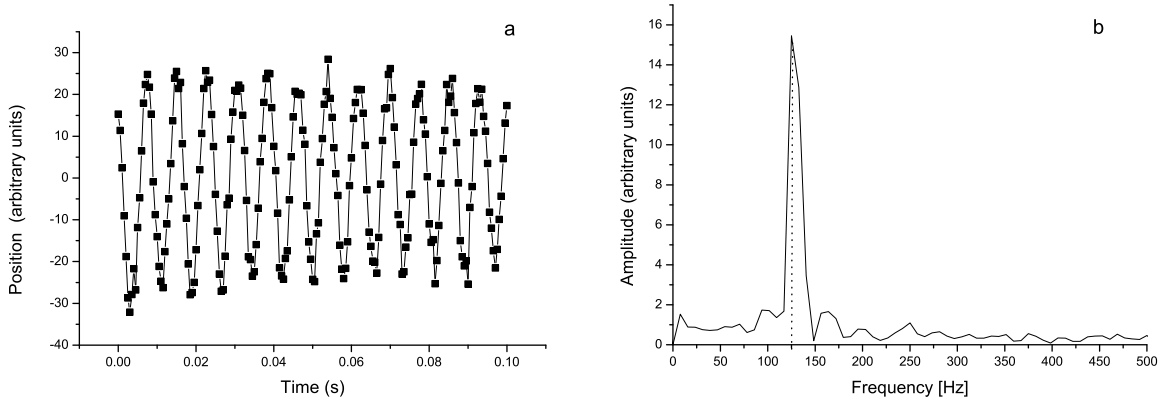

Figure 6.4: Axial trap frequency: a) shows the position of the cloud which changes due to the center of mass motion; b) is the fast Fourier transformation of the data point, yielding a peak at a frequency $\omega = 2\pi\times$ 128 Hz.

agreement with the calculated trap frequency of $2\pi\times35$ Hz. We attribute this to the coarseness of the magnetic structure, due to the fabrication process. We found, after cooling the cloud, that the potential exhibits a strong field corrugation leading to two separate minima with a magnetic field zero in the lower minimum. This can also be seen in Figure 6.5. Because the applied rf knife lasts longer than its life time, this zero minimum disappears and we are left only with one of the traps.

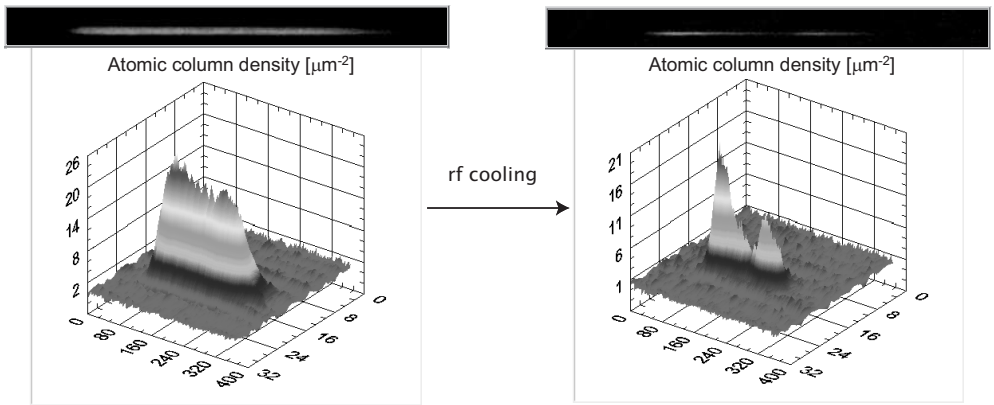

Figure 6.5: Atom column density of the cold cloud close to the surface, before cooling (a) and after cooling (b).

Radial frequency

To measure the radial frequency the trap is shaken at an appropriate frequency and due to parametric heating (when the modulation frequency matches the trap

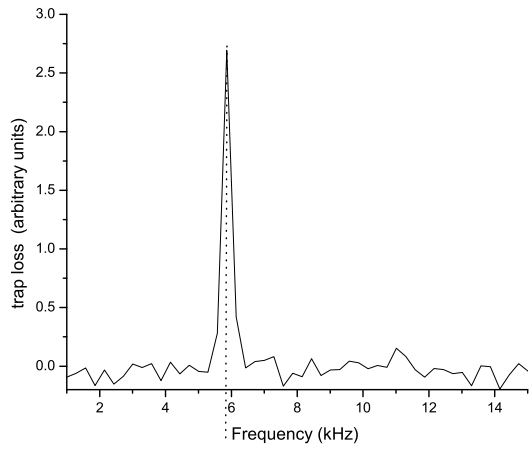

Figure 6.6: Radial frequency measured by modulating the trap at an appropriate frequency. Frequency peak at 5.8 kHz.

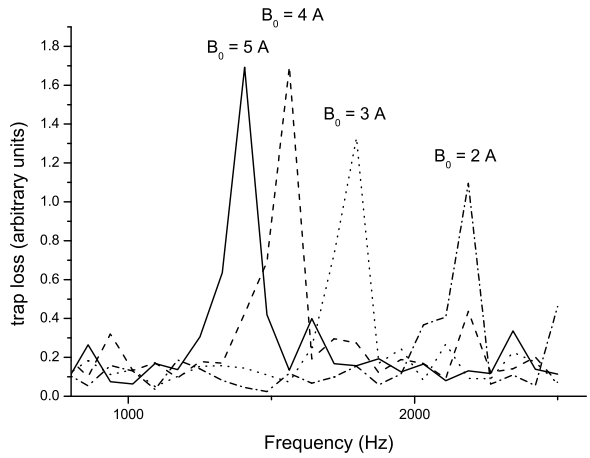

Figure 6.7: Direct observation of the radial frequency by shaking the trap center and for different values of applied axial fields, given here as the currents (5, 4, 3, and 2 A) sent through the MT coils (see Sec. 3.3).

frequency) atom loss can be observed [87]. The heating is typically accompanied by a loss of atoms due to plain evaporation.

We measured the trap loss as a function of modulation frequency. The best fit gives us a frequency of $\omega_r = 2\pi\times5.8$ kHz, as plotted in Figure 6.6. This value is not in agreement to our simulated results ($\omega_r = 2\pi\times11$ kHz) as the radial frequency depends on the minimum field B_0. Therefore we also performed frequency measurements for different trap bottoms. For this we measured the trap loss as a function of the shaking frequency for different B_0. The results are

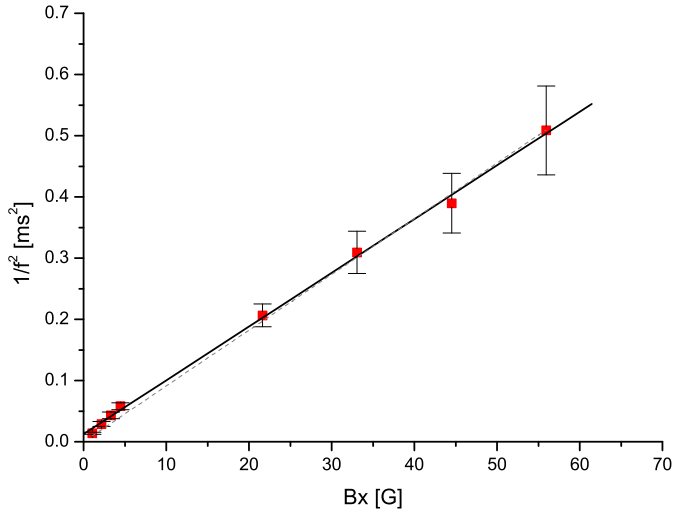

Figure 6.8: The radial frequency dependence on the bias field. We plot the frequency $1/f^2$ vs. the axial applied field B_x. The solid line is a linear fit to the data.

shown in Figure 6.7.

The expected dependence is $1/f^2 = 4\pi^2 m B_0/m_F g_F \mu_B B'^2$, and it is used to calculate the offset magnetic field in the center of the trap, B = 2.7 G (see Figure 6.8). Knowing the trap frequencies and the measured B we can then calculate the trap gradient $\sim$ 85 T/m. It is close to the simulated value ($\sim$ 90 T/m). The small difference may be caused by the geometry that can be slightly different than designed and the surface coarseness.

6.3 Conclusions

We have demonstrated that a Ioffe-Pritchard trap can be created on a fully permanent magnetic atom chip, where we could trap $\sim 2 \times 10^6$ atoms. We have described the non trivial loading procedure of a purely magnetic chip. This relies on the adiabatic movement of Ioffe trap using uniform external fields and making use of the forced evaporative cooling during loading. The in-trap analysis of an ultracold atom cloud, confined using a purely permanent magnetic atom chip, and its difficulties are as well presented here. The temperature of the cloud is inferred from the axial size of the cloud by observing the in-situ atomic density distribution. We have reached the critical temperature and observed degeneracy (phase-space density > 1).

The measurement of the trap gradient shows us that the simulated magneti-

zation it is not far from what we actually measured.

We also observed that the potential exhibits a strong field corrugation leading to two separate minima with a magnetic field zero in the lower minimum. This leads to short lifetimes $\sim$ 200 ms. This can happen due to the coarseness of the magnetic structure produced during the fabrication process. Therefore, the measured frequencies - $\omega_a = 2\pi\times$ 128 Hz, $\omega_r = 2\pi\times$ 5.8 kHz - are different then the calculated ones. These field zeroes were lifted by placing a permanent magnet on the optical table.